# Fast generic method for force gradient evaluation and data averaging in force spectroscopy techniques

Layla Bou Tannous, Audrey Steinberger

# Fast generic method for force gradient evaluation and data averaging in force spectroscopy techniques

Layla Bou Tannous[†,‡] and Audrey Steinberger[*,¶]

†*Laboratoire de Chimie, École Normale Supérieure de Lyon & CNRS, 69364 Lyon, France*
‡*Univ. Grenoble Alpes, CEA, Leti , F-38000 Grenoble, France*
¶*CNRS, ENS de Lyon, LPENSL, UMR5672, 69342, Lyon cedex 07, France*

E-mail: audrey.steinberger@ens-lyon.fr

## Abstract

Force spectroscopy enables the experimental study of intermolecular and surface forces from molecular biology to hard material science, by measuring the interaction force versus the distance between the surfaces, called the separation. However, analyzing large datasets remains challenging. Here, we introduce a robust and fast method leveraging separation histograms to evaluate force gradients and average force profiles in force spectroscopy data. In experiments with constant driving velocity, an affine relationship between the separation histogram and the force gradient is demonstrated, enabling the reconstruction of force-separation profiles with even spatial resolution and reduced noise. Additionally, two efficient averaging schemes are proposed, based on the cumulative separation histogram of a dataset and outperforming a conventional interpolation method. The procedures are illustrated with data obtained at the interface between an ionic liquid and a solid substrate by Atomic Force Microscopy, but are generic to all kinds of force spectroscopy techniques and systems.

## Keywords

Force spectroscopy, separation histograms, force gradient reconstruction, data averaging, high-throughput analysis

Force spectroscopy is a powerful way to investigate intermolecular and surface forces by directly measuring the interaction force $F$ between two surfaces as a function of their separation distance $h$.[1] Applications go from hard material science to physical chemistry and biology. It enables to study long-range electrostatic forces between two surfaces,[2,3] as well as the short-range ordering of a liquid close to a solid surface.[4–9] Moreover, it is widely used to study the mechanical properties and adhesion of various substrates, including polymer coatings, lipid bilayers and biological tissues.[10–12] Single molecule spectroscopy of the folding/unfolding and the adhesion of polymers and long biomolecules can also be characterized by tethering the surfaces with the molecule of interest.[13,14]

Force spectroscopy measurements can be performed using well-established experimental techniques such as optical tweezers,[15] Surface Force Apparatus (SFA),[16] and Atomic Force Microscopy (AFM).[17] All these techniques are modeled the same way: one of the surfaces is attached to an elastic element that acts as a spring of stiffness $k$. When the spring is in mechanical equilibrium, its deformation $d$ gives a

restoring force $-kd$ exactly opposing the interaction force $F$ acting on the attached surface due to the opposing surface, as illustrated in Figure 1; then $F = kd$. To vary the separation $h$ between the two surfaces, either the base of the spring or the opposing surface is moved by a distance $z$ perpendicularly to the surfaces. The separation $h(t)$ is then equal to:

$$h(t) = z(t) - z_0 + d(t) = z(t) - z_0 + \frac{F(t)}{k}, \quad (1)$$

where $z_0$ is a constant distance defining the origin of the separation axis. Beware that the value of $z_0$ differs slightly in each experimental run due to thermal drifts. It also varies along the surface because it depends on its topography. In practice, $z_0$ is often deduced from the shape of each experimental curve.

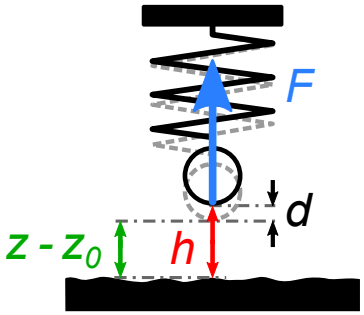


Figure 1: Generic sketch of a force spectroscopy experiment. The force $F$ acting on the probe deflects the spring by the distance $d$ with a probe-surface separation $h$. The shape of the undeflected spring is represented in gray dashed lines. The distance $z$ is varied using a piezoelectric element (not depicted). In mechanical equilibrium, the restoring force of the spring opposes the force $F$ so that $F = kd$, where $k$ is the stiffness of the spring.

In many systems, obtaining statistically relevant results requires compiling the results of a large number of force curves.[12,18] A bivariate histogram, also called 2D histogram, is an efficient visual rendering of a large set of force curves by color-coding the total number of data points that fall into each rectangular force-separation bin,[5] as shown in the right panel of Figure 2. Besides, this statistical representation allows to identify small reproducible features buried under thermal and measurement noise in single profiles.[9] However, 1D curves are often more convenient than 2D pictures *e.g.* for data fitting or for overlaying different data sets. Yet, computing an average force profile for force spectroscopy measurements is not straightforward, because each force vector is acquired over a different $z - z_0$ distance vector even for identical acquisition parameters, because of the variation of $z_0$ (see Supplementary Information Figure S4 for an example).

In this framework, the cumulative separation histogram of a series of force-separation curves has been shown to be a convenient tool to study the local layering of an ionic liquid close to a solid substrate in sharp tip AFM experiments. Indeed the distance between the local maxima of the histogram corresponds to the average distance between the successive ionic layers. Since the seminal works by Black et al.[6] and Cheng et al.[7] in 2015, this very useful, robust, and easy to compute representation has been spreading in the ionic liquid community. It has also been used for advanced analysis of single SFA force-separation curves.[8] But what exactly are separation histograms?

A separation histogram counts the number $n(\mathtt{h})$ of data points that belong to the bin of width $\Delta h$ centered around the separation $\mathtt{h}$. The choice of $\Delta h$ defines the spatial resolution of the subsequent analysis. The time $\Delta t$ spent in a small interval $\Delta h$ can be evaluated using the time derivative of equation 1:

$$\frac{\Delta h}{\Delta t} \simeq \frac{\partial h}{\partial t} = \frac{\partial z}{\partial t} + \frac{1}{k}\frac{\partial F}{\partial t} = \frac{\partial z}{\partial t} + \frac{1}{k}\frac{\partial F}{\partial h}\frac{\partial h}{\partial t}. \quad (2)$$

Therefore, if an approach (or retraction) is realized at a constant velocity $V$ so that $z = Vt$, with a constant sampling rate $f_s$, the number of points $n(\mathtt{h})$ is a simple affine function of the force gradient $F' = \frac{\partial F}{\partial h}$:

$$n(\mathtt{h}) = f_s \Delta t \simeq \frac{f_s \Delta h}{V}\left(1 - \frac{1}{k}F'(\mathtt{h})\right). \quad (3)$$

As a result, the force gradient can be easily

computed from the 1D separation histogram:

$$F'(\mathtt{h}) \simeq k\left(1 - \frac{n(\mathtt{h})}{n_0}\right), \qquad (4)$$

with a resolution that is controlled by the factor $n_0 = \frac{f_s \Delta h}{V}$. $n_0$ can be computed directly from the values of $V$, $f_s$ and $\Delta h$, or as the mean value of $n$ in a region where the force gradient is equal to zero, typically far from the mechanical contact. For a given spatial resolution $\Delta h$, the experimental parameters $V$ and $f_s$ should be chosen so that the factor $n_0$ is larger than 1. The fact that the force gradient $F'$ cannot be larger than $k$ due to the mechanical instability of the spring[1] coincides with the fact that the number of data points $n$ cannot be smaller that zero.

The force profile can then be reconstructed over the separation vector $\mathtt{h}$ by integrating $F'(\mathtt{h})$, starting from a separation where the force is equal to zero (usually at large separations). The detailed integration procedure is discussed in the Supplementary Information, comparing two slightly different Matlab implementations that are both included in the Supporting Information. On a single force curve, this reconstruction is useful to check the validity of equation 4 and locate where it fails due to the finite force setpoint, or unsuitable acquisition parameters. Moreover, as the force is reconstructed over an evenly-spaced separation vector, data points are added in regions of the force-separation profile where the measured ones are scarce due to sharp force variations, forming a straight line with a slope equal to $k$ over a jump due to the mechanical instability of the spring. Another advantage is that the reconstruction procedure smooths out the thermal noise.

This method is illustrated for a single force profile in the left column of Figure 2, using AFM approach curves acquired in the ionic liquid 1-butyl-3-methylimidazolium bis(trifluoromethanesulfonyl) ($C_4$mimN$Tf_2$) on mica, with a silicon cantilever of stiffness $k = 0.25\,\mathrm{N\,m^{-1}}$ equipped with a sharp tip, following the experimental procedure described in Bou Tannous et al.[9] (see the Supporting Information for more experimental details). The bottom plot shows the separation histogram and the force gradient computed from equation 4 corresponding to the experimental force-separation curve represented in red circles in the top plot. The local minima in these plots correspond to layer ejection events (see the Supporting Information for a detailed description of these layers). Here the acquisition frequency is $f_s = 2048\,\mathrm{Hz}$, the measured driving velocity is $V = 62.3\,\mathrm{nm\,s^{-1}}$, and the width of the separation bin is $\Delta h = 0.05\,\mathrm{nm}$, in agreement with the average number of data points per separation bin measured between 10 and 30 nm: $n_0 = 1.643$. On the top plot, the force profile reconstructed by integrating $F'$ matches very well the experimental one at separations larger than the leftmost maximum in the separation histogram, proving the validity of equation 4 in that region. For lower separations, relation 4 is no longer valid because the number of points in the histogram drops due to the finite force setpoint. In the reconstructed profile, data points are added in the regions between 0.7 and 1.1 nm and between 1.6 and 2.05 nm, where ionic layers are ejected.

Interestingly, the same procedure can be applied on a series of $m$ force curves, as shown in the right column of Figure 2 for $m = 50$ successive approach curves in the same experimental system. The average force gradient can be easily computed from their cumulative separation histogram using equation 4, with $n_0$ the average number of points in a region where $F' = 0$ (bottom plot).

Furthermore, from the computation of the cumulative separation histogram, averaging the force-separation curves together becomes straightforward. We propose two very efficient methods. The first one is simply integrating the average force gradient, as was done for the single force curve. In the top right plot of Figure 2, the resulting average force profile $F_{\mathrm{cumsum}}$ is superposed on the 2D force-separation histogram for the set of 50 experimental curves. Beware that this method is only valid for experiments performed with a saw-tooth $z$ displacement profile as it relies on equation 4. The second method is applying the sorting pattern of the

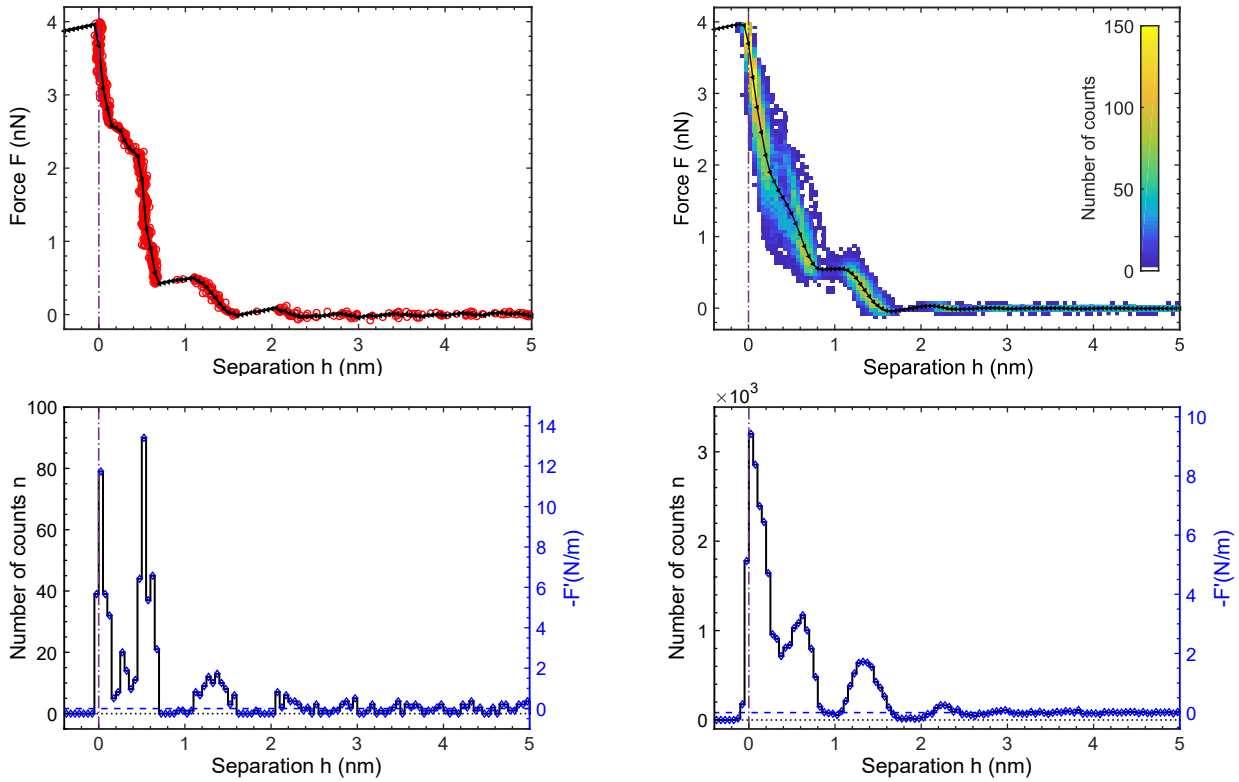


Figure 2: Force versus separation curves (top figures), and corresponding separation histograms (bottom figures) for 1 AFM approach curve (left column), and 50 approach curves (right column) in $C_4$mimNTf$_2$ on mica. Top figures: (left) the experimental points are represented as red circles, (right) the 50 experimental curves are represented as a 2D force-separation histogram, where the total number of data points in each force-separation bin is color-coded according to the colorbar in inset, with a bin size of $\Delta h = 0.05\,\text{nm}$ and $\Delta F = 0.05\,\text{nN}$. In both figures, the black line with triangle markers correspond to the force profile obtained by integrating $F'$ computed using eq. 4. Bottom figures: separation histogram (black line) and opposite of the force gradient $F'$ computed with eq. 4 (blue diamonds). The dashed line locates $n = n_0$ and $F' = 0$. The dotted line locates $n = 0$ and $-F' = -k$. The vertical dashed-dotted line locates the leftmost maximum in the separation histogram.

separation data to the force data, and simply averaging together the force data that belong to the same separation bin. Note that this sorting method is completely generic: it works with any kind of repeated piezo displacement profiles (sinusoidal,...), and with any type of data plotted against the separation (frequency of phase shift, excitation or oscillation amplitude,...).

In Figure 3, the average force profiles $F_{\text{cumsum}}$ from the integration of the average force gradient and $F_{\text{median}}$, the median value of the force data sorted along the separation bins, are compared to the force profile $F_{\text{interpZ}}$ obtained using a conventional averaging scheme. The conventional scheme[19] computes the median force value after interpolating the forces over a common distance vector $z - z_0$ to deal with the differing $z_0$, then deduces the associated separation $h$ from the chosen distance vector and the average force $F_{\text{interpZ}}$ using equation 1. Computational details for the three averaging schemes are given in the Supplementary Information and Matlab implementations are included in the Supporting Information. Overlaying these force profiles on top of the 2D histogram shows that all three methods give a very good but slightly different representation of the average force profile. As expected, the two histogram-

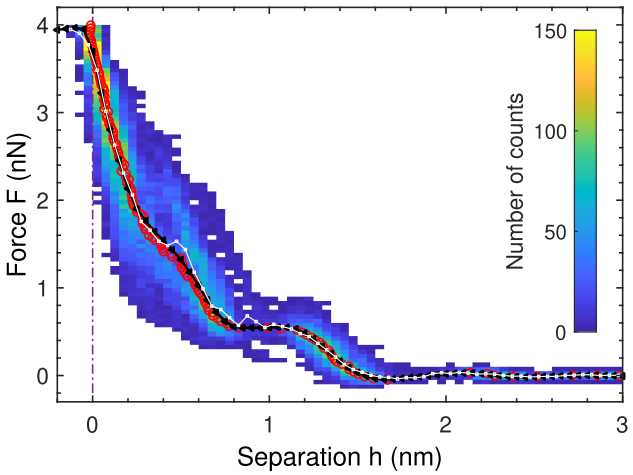


Figure 3: Comparison of three averaging schemes tested on 50 AFM approach curves in $C_4$mimNT$f_2$ on mica, displayed as a 2D force-separation histogram as in the right column of Figure 2. Black line with triangle markers: force profile $F_{\text{cumsum}}$ obtained by integrating $F'$ computed using eq. 4. White line with square markers: average force profile $F_{\text{median}}$ obtained by computing the median of the force data sorted along the bins of the separation histograms. Red circles: average force profile $F_{\text{interpZ}}$ obtained by averaging the forces after interpolating them over a common distance vector $z-z_0$. The separation vector $h$ in the $x-$axis is then computed from $z - z_0$ and the average force using equation 1. The vertical dashed-dotted line locates the leftmost maximum in the cumulative separation histogram (Figure 2, bottom right).

based methods fail for separations lower than the leftmost maximum in the cumulative separation histogram and should not be exploited in that region. $F_{\text{cumsum}}$ and $F_{\text{interpZ}}$ are in excellent agreement, which fully validates the evaluation of average force gradient. However, $F_{\text{median}}$ differs from the two other curves in the layer ejection regions. Indeed by construction, the slope between adjacent points is constrained to remain below $k$ in $F_{\text{cumsum}}$ and $F_{\text{interpZ}}$ (as in individual experimental force curves), while there is no such constraint in the data sorting method. As a result, $F_{\text{median}}$ can follow more closely the crest line of the 2D histogram around 5 nm, just before the ejection of the inner ionic layer, than the other two average profiles, but is less smooth than $F_{\text{cumsum}}$ in the layer ejection regions where there is a low number of data points due to mechanical instability. Note that in these regions, there is no data points for the conventional average $F_{\text{interpZ}}$. There are two main advantages of the histogram-based averaging schemes over the conventional one. First, they are built over an evenly-spaced and user-defined separation vector, whereas $F_{\text{interpZ}}$ is defined over an unevenly-spaced separation that is specific to the corresponding data set. Last but not least, the sorting procedure is twice faster than the conventional one, while the integration procedure (including the computation of the cumulative histogram) is more than 30× faster than the conventional one, resulting in a significant gain in computational efficiency.

To conclude, taking benefit from the separation histogram opens a powerful and efficient data analysis toolbox for all kinds of force spectroscopy techniques. For quasi-static experiments performed with a saw-tooth $z$ displacement profile, the force gradient of a single force-separation curve can be easily evaluated from its affine relationship with the separation histogram, with neither smoothing nor fitting of the data. It can then be used *e.g.* to automatically detect rupture events in a large number of force curves obtained by AFM[20,21] and optical tweezers.[22] Furthermore, integrating the force gradient reconstructs the force profiles over a user-chosen and evenly-spaced separation vector and smooths out the thermal noise, facilitating a quantitative comparison between several curves such as approach and retraction profiles. Likewise, applying the same procedure from the cumulative separation histogram of a series of experimental curves yields the average force gradient and an average force profile. Alternatively, the computation of the cumulative histogram provides a sorting pattern than can be used for computing the average profile of any kind of data plotted against the separation $h$, for any kind of repeated $z$ displacement. Therefore, this strategy can also be applied in dynamic force spectroscopy experiments, when the spring is oscillated and dynamic quantities such as the oscillation amplitude are recorded.

Finally, when averaging a large number of data sets, replacing numerous interpolations by the evaluation of a single histogram allows a major gain in computational efficiency.

**Acknowledgement** The authors thank the Agence Nationale de la Recherche for supporting financially this work (Grant No. ANR-18-CE09-0018). They also thank C. Cottin-Bizonne and A. Piednoir for critical reading of the manuscript.

# Supporting Information Available

Detailed description of the experimental procedure and layering of the ionic liquid, data treatment, numerical implementation of the force gradient computation and of the averaging procedures, and detailed comparison of averaging schemes (PDF). Corresponding Matlab functions are also given as Supporting Information (ZIP).

# References

(1) Israelachvili, J. N. *Intermolecular and surface forces*, 3rd ed.; Academic Press: Burlington, Massachusetts, 2011.

(2) Rotsch, C.; Radmacher, M. Mapping Local Electrostatic Forces with the Atomic Force Microscope. *Langmuir* **1997**, *13*, 2825–2832.

(3) Mohideen, U.; Roy, A. Precision Measurement of the Casimir Force from 0.1 to 0.9$\mu$m. *Physical Review Letters* **1998**, *81*, 4549–4552.

(4) Israelachvili, J. N.; Pashley, R. M. Molecular layering of water at surfaces and origin of repulsive hydration forces. *Nature* **1983**, *306*, 249–250.

(5) Black, J. M.; Walters, D.; Labuda, A.; Feng, G.; Hillesheim, P. C.; Dai, S.; Cummings, P. T.; Kalinin, S. V.; Proksch, R.; Balke, N. Bias-Dependent Molecular-Level Structure of Electrical Double Layer in Ionic Liquid on Graphite. *Nano Letters* **2013**, *13*, 5954–5960, PMID: 24215396.

(6) Black, J. M.; Baris Okatan, M.; Feng, G.; Cummings, P. T.; Kalinin, S. V.; Balke, N. Topological defects in electric double layers of ionic liquids at carbon interfaces. *Nano Energy* **2015**, *15*, 737–745.

(7) Cheng, H.-W.; Stock, P.; Moeremans, B.; Baimpos, T.; Banquy, X.; Renner, F. U.; Valtiner, M. Characterizing the Influence of Water on Charging and Layering at Electrified Ionic-Liquid/Solid Interfaces. *Advanced Materials Interfaces* **2015**, *2*, 1500159.

(8) Griffin, L. R.; Browning, K. L.; Clarke, S. M.; Smith, A. M.; Perkin, S.; Skoda, M. W. A.; Norman, S. E. Direct measurements of ionic liquid layering at a single mica–liquid interface and in nano-films between two mica–liquid interfaces. *Physical Chemistry Chemical Physics* **2017**, *19*, 297–304.

(9) Bou Tannous, L.; Simoes Santos, M.; Gong, Z.; Haumesser, P.-H.; Benayad, A.; Padua, A. A. H.; Steinberger, A. Effect of Surface Chemistry on the Electrical Double Layer in a Long-Chain Ionic Liquid. *Langmuir* **2023**, *39*, 16785–16796.

(10) Burnham, N. A.; Colton, R. J. Measuring the nanomechanical properties and surface forces of materials using an atomic force microscope. *Journal of Vacuum Science & Technology A* **1989**, *7*, 2906–2913.

(11) McConney, M. E.; Singamaneni, S.; Tsukruk, V. V. Probing Soft Matter with the Atomic Force Microscopies: Imaging and Force Spectroscopy. *Polymer Reviews* **2010**, *50*, 235–286.

(12) Olubowale, O. H.; Biswas, S.; Azom, G.; Prather, B. L.; Owoso, S. D.; Rinee, K. C.; Marroquin, K.; Gates, K. A.; Chambers, M. B.; Xu, A.; Garno, J. C. "May the

Force Be with You!" Force–Volume Mapping with Atomic Force Microscopy. *ACS Omega* **2021**, *6*, 25860–25875.

(13) Janshoff, A.; Neitzert, M.; Oberdörfer, Y.; Fuchs, H. Force Spectroscopy of Molecular Systems—Single Molecule Spectroscopy of Polymers and Biomolecules. *Angewandte Chemie International Edition* **2000**, *39*, 3212–3237.

(14) Ritort, F. Single-molecule experiments in biological physics: methods and applications. *Journal of Physics: Condensed Matter* **2006**, *18*, R531.

(15) Gieseler, J.; Gomez-Solano, J. R.; Magazzù, A.; Castillo, I. P.; García, L. P.; Gironella-Torrent, M.; Viader-Godoy, X.; Ritort, F.; Pesce, G.; Arzola, A. V.; Volke-Sepúlveda, K.; Volpe, G. Optical tweezers — from calibration to applications: a tutorial. *Advances in Optics and Photonics* **2021**, *13*, 74–241.

(16) Hayler, H. J.; Groves, T. S.; Guerrini, A.; Southam, A.; Zheng, W.; Perkin, S. The surface force balance: direct measurement of interactions in fluids and soft matter. *Reports on Progress in Physics* **2024**, *87*, 046601.

(17) Butt, H.-J.; Cappella, B.; Kappl, M. Force measurements with the atomic force microscope: Technique, interpretation and applications. *Surface Science Reports* **2005**, *59*, 1–152.

(18) Bosshart, P. D.; Casagrande, F.; Frederix, P. L. T. M.; Ratera, M.; Bippes, C. A.; Müller, D. J.; Palacin, M.; Engel, A.; Fotiadis, D. High-throughput single-molecule force spectroscopy for membrane proteins. *Nanotechnology* **2008**, *19*, 384014.

(19) Sokolov, I.; Kalaparthi, V.; Kreshchuk, M.; Dokukin, M. On averaging force curves over heterogeneous surfaces in atomic force microscopy. *Ultramicroscopy* **2012**, *121*, 16–24.

(20) Odorico, M.; Teulon, J.-M.; Berthoumieu, O.; w.W. Chen, S.; Parot, P.; Pellequer, J.-L. An integrated methodology for data processing in dynamic force spectroscopy of ligand–receptor binding. *Ultramicroscopy* **2007**, *107*, 887–894.

(21) Li, J.; Sullan, R. M.; Zou, S. Atomic Force Microscopy Force Mapping in the Study of Supported Lipid Bilayers. *Langmuir* **2011**, *27*, 1308–13.

(22) Buck, S.; Pekarek, L.; Caliskan, N. POTATO: Automated pipeline for batch analysis of optical tweezers data. *Biophysical Journal* **2022**, *121*, 2830–2839.

# TOC Graphic

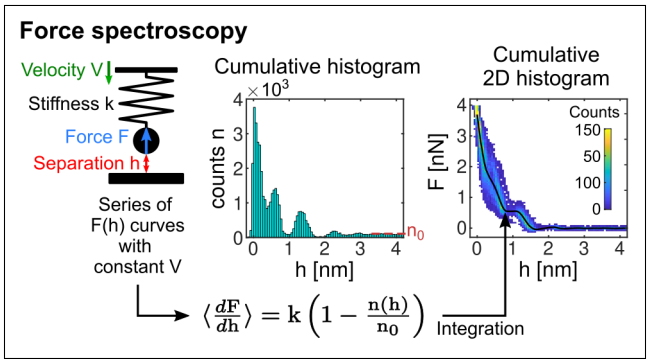
Force spectroscopy
Velocity V
Stiffness k
Force F
Separation h
Series of F(h) curves with constant V
Cumulative histogram
counts n
h [nm]
Cumulative 2D histogram
F [nN]
Counts
150
50
100
0
h [nm]
Integration